POLITECNICO
DI TORINO

Université
de Paris

Master's double degree in Nanotechnologies and Quantum Devices

Master's Thesis

High Power InP MOPA for LiDAR and Free Space Optical communications

Supervisors
Prof. Carlo Ricciardi
Prof. Maria Luisa Della Rocca

Candidate
Andrea Demarchi

Supervisor
III-V Lab
Dr. François Duport

July 2020

Abstract

Master Oscillator Power Amplifiers (MOPAs) are III-V semiconductor based monolithically integrated optoelectronic sources, that are studied as application for Light Detection and Ranging and Free Space Optical communications. MOPAs enable the possibility to have a modulated signal, together with a high output power. A study on the mode confinement inside the Slab Coupled Optical Waveguide structure is presented, in order to maximize the device output power; together with it a theoretical and numerical study on the impact of optical nonlinearities on gain and phase dynamics and on power and gain along the length of the Semiconductor Optical Amplifier output stage is developed, to address the possibility to have amplitude and phase modulation from the SOA output stage.

Acknowledgements

A very special acknowledgement is addressed to my internship supervisor, Dr. François Duport, who followed me in this experience, and was always ready to teach me new things and to discuss about my doubts during the work.

Together with him, my thanks go to his colleagues and to all the members of the research group, in particular to Dr. Frédéric Van Dijk, for the effort he spent to give me the best possibilities in the following.

I want also to thank all the institutions involved in my education, that gave me the very useful knowledge in the field.

I want to thank all my friends, who never left me alone and with whom I passed lot of beautiful moments; with them my mates, for the time passed together during the internship.

Finally, I want to dedicate this work to my parents and my family, for all the efforts they have done throughout the years, to give me the possibility to reach this important step in my life and education, helping me for any kind of issue.

Contents

Chapter 1

Introduction

1.1 MOPAs for LiDAR and Free Space Communications

Satellite-to-satellite or satellite-to-ground communications have been dependent up to now on RF communications; these latter, due to the weight and dimensions of devices, together with their power consumption, are now too demanding to be employed on satellite systems, that have low power availability and cannot sustain high weights. Another limit of RF communications are the rules concerning the usage of the RF frequency band, that reduce the possibilities of evolution for this kind of systems. Even if for some kinds of satellites RF communications remain the only implementation, big advantages instead are given by optical communications; thus, in order to have space communications transmitting more than Gb/s, 'Free Space Optical communications' or FSO have become a good alternative. FSO considers not only optical links for space applications (that require from hundreds to millions of kilometers), but also atmospheric transmissions (emitter and receiver are both in the atmosphere) that require a maximum of 100 kilometers, and data centers internal transmissions that require very fast transfer (Tb/s) at a reduced distance (some meters, [7]). In the framework of satellite-to-satellite communications, III-V semiconductor based optical sources play an important role for their low weight, their lower power consumption and the possibility to transmit optical information. Another application of interest for these devices is 'LIght Detection And Ranging' (LiDAR), that has as objective the measurement of gas concentrations in the atmosphere by means of differential absorption (DIAL LiDAR); the measurement is performed satellite-to-ground in this case. For both applications, the employed optical sources have to ensure almost $1\,W$ of output power in order to cover the long distances in between transmitters and receivers, and to provide a correct transmission of information without degradation; this latter can be very high in the atmosphere (almost $30\,dB$), due to absorption and scintillation phenomena.
In between the different available optical sources, monolithically integrated MOPAs or 'Master Oscillator Power Amplifiers' can ensure an high output power, together with modulation capabilities, given by the possibility to integrate on the same chip a semiconductor laser ('MO'), a modulator and a semiconductor optical amplifier ('PA'), in the particular case of the following work. The possibility to amplify and to modulate the signal in the same device enables both to ensure a good power transmission and to transmit the correct information. The three sections of the device are current driven, and light is emitted by stimulated emission in the device through the population inversion which is achieved in the material, thanks to current pumping.
The following work, which is in the framework of a five months internship, that was intended at the beginning to be an experimental study of the modulation capabilities of the device,

then shifted into a theoretical work both on the study of the modal propagation inside the structure (in order to obtain the best structure that maximizes the output power), and on the theoretical evaluation of the effects of optical nonlinearities in the HP-SOA stage, together with a related numerical model. This latter part evaluates the possibility to use the SOA stage also for the phase modulation of the signal (something that in the integrated MOPA presented before was part of the modulator stage).

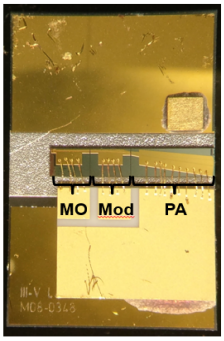

(a) MOPA considered in the following: a modulator is added in between the 'MO' and the 'PA' stages.

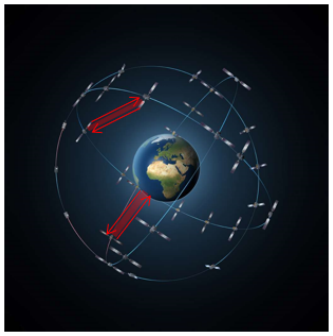

(b) Satellite-to-satellite FSO communication

Figure 1.1: Solid state based MOPA considered in the work - Representation of FSO

1.2 Presentation of the Lab and of the team

The following work is part of an internship on the same subject at III-V Lab, which is a private research lab set-up between Thales, Nokia Bell Labs and CEA-Leti. The purpose of the lab is to focus on the development of III-V semiconductor based technologies and their integration with Silicon circuits and micro-systems. Applications are in optical and wireless networks for communication technologies, defense, security, space, aerospace, transportation and exploitation for high volume applications. Epitaxy, processing, testing and modelling of devices all take place in the lab; in particular, 2000 m^2 of clean room are availables.
The 'Optoelectronic Sources Group', that has at its head Dr. Frédéric Van Dijk and is composed by Dr. François Duport and Dr. Michel Krakowski, in which the following work has been carried out, concentrates its activities on III-V semiconductor based components for high frequency photonic applications. Its main activities are on analog signal distribution on fibre for RADAR systems, semiconductor lasers for short pulse generation, semiconductor components for RF signal generation and lasers with low linewidth for LiDAR applications. One of the most important objectives of the group is to reproduce in the optical domain for LiDAR applications what is already present in the RF domain for RADAR applications. Together with MOPAs, the group focuses its attentions on Photonic Integrated Circuits based optical sources, and on hybrid integrated InP-based systems on silicon that have as main applications the development of optoelectronic oscillators or low linewidth lasers based on bragg gratings and ring filters. With hybrid components, nonlinear optical applications are studied, as for example micro-resonator based frequency combs.

Chapter 2

Presentation of the internship subject

2.1 State of the art

Master Oscillator Power Amplifiers are optical systems consisting in the series of a master laser, that provides the input signal at a precise wavelength, and an optical amplifier, that amplifies the input signal at the output of the device. Different implementations are possible, depending on the kind of devices employed, and on the possibility to have a discrete or an integrated system. One possible implementation of the MOPA is the fibre-based one (see as an example [15]), that employs fibre-based blocks and optics to couple them: fibre-based devices show high optical losses and high noise factors, that reduce the overall gain. They also require high volume and weight together with high input power, something which is not preferable when all the system has to be embedded on satellites, that could provide little power and not enough space, and cannot sustain so much weight. Semiconductor based devices instead could solve most of these issues in terms of volume and weight, and if they are monolithically integrated, they can reduce losses (no coupling optics is needed), leading to an higher overall gain in the device, so to an higher output power. Moreover, solid state based sources are less affected by radiations with respect to the fibre-based counterpart; this turns out to be very important in space applications in which radiations play an important role. Instead, solid state based sources are not advantaged with respect to fibre-based ones for what concerns temperature effects; a tradeoff has to be done between the decrease of size and the thermal management of the device. Semiconductor based MOPAs can be produced both for commercial or experimental purpose. In general, for commercial applications, MOPAs are produced in different separated subunits; very few examples of industries selling semiconductor based MOPAs monolithically integrated are present. One of these is QPC Lasers, that sells monolithically integrated lasers and evased SOA with output powers in the range $1 - 1.5\,W$ emitting at wavelength from 1550 to $976\,nm$ [7]. For what concerns MOPAs for research purposes, they can be hybrid (having the different parts separated and optically coupled) or monolithically integrated on the same chip. Different examples of hybrid MOPAs have as source DBR ('Distributed Bragg Reflector') or DFB ('Distributed Feedback') lasers; the first ones, having a more complicated structure, require more sections (so more volume) than DFBs; they all have a monomode emission with a high SMSR ('Single Mode Suppression Ratio') of dozens of dB. In the case of hybrid MOPAs, the source is then coupled to the amplifier by means of Graded Index cylindrical lenses. In the case of monolithically integrated MOPAs, the length of the source (DFB or DBR) has to be fixed at a maximum of $4\,mm$, and the SOA stage consists only in the evased part because there are no optical losses between the different stages of the MOPA. An

interesting case of monolithically integrated MOPA is the one from Freedom Photonics ([14]), which has a 2 QW-based active region and 2.5 W of output power.

2.2 The structure of monolithically integrated MOPA

The MOPA under study consists in the monolithic integration of a DFB laser, that provides the emission of light with a very good spectral quality, an HP-SOA, that amplifies the signal conserving spectral purity; in between of them a modulator is integrated, that enables the possibility to modulate the amplitude of the signal externally, in order to generate a digital signal. The three stages of the device (as shown in 2.2) share the same vertical structure which is the Slab Coupled Optical Waveguide (SCOW) architecture [13]. The structure is grown on a n-doped InP substrate; the active region consists on a multi quantum well (MQW) structure of six 8 nm-wide quantum wells separated by seven 10 nm-wide barriers. The optical waveguide is based on a 5 μm-thick large ridge structure with a thick 4 μm optical slab of GaInAsP. The upper part of the waveguide cladding is made on semi-insulating Fe-doped InP thanks to the Semi Insulating Buried Heterostructure (SIBH) technique. A layer of p-doped InP is then the upper part of the cladding (2.1b). The use of InP provides the emission at $\lambda = 1.55\,\mu m$; this is also ensured by the use of InGaAsP quaternaries with adjusted concentrations in the active region, that have a good lattice matching for the epitaxial structure growth. The InGaAsP alloys employed in the active region will be denoted for simplicity 'Q1.17' where 1.17 stands for the 1.17 μm of wavelength equivalent to the energy gap of the material. The MQW active region, due to its 2-d nature, shows a constant density of states for each single energetic level and becomes a ladder-like curve considering N levels; this reduces the laser threshold current, because the maximum gain is achieved for a lower density of states, something that cannot happen in a bulk (3-d) semiconductor material. To improve the maximum obtainable gain, and to choose the right polarization for the emitted light, the quantum wells in the active region are in compressive strain, because this latter affects the effective mass of light holes and heavy holes in the valence band ([7]). The mode that propagates inside the SCOW structure is thus vertically guided by the refractive index gradient between the MQW active region and the waveguide cladding. The horizontal guiding of the mode is achieved thanks to the adopted SIBH technique, employing the barriers created by the Fe-doped InP. Together with the horizontal confinement, a good improvement in the performances of the device can be achieved by concentrating the carrier injection inside the region in which the mode is more confined; this is technologically achieved by implantation of protons in the p-doped region above the Fe-doped InP barrier, that reduces current leakages in the sections in which the mode is not confined. Thanks to the SCOW architecture, that introduces the n-doped slab below the active region with an intermediate refractive index, the mode is shifted down in the waveguide, reducing the overall losses in the device, that have their main contributions coming from the upper p-doped region (the mechanism of loss in the different part of the waveguide will be described later in details); another possibility is based on lowering the thicknesses of the two Separate Confinement Heterostructure (SCH) layers. These latter, are two layers made of InGaAsP Q1.17, that are above and below the active region; they also have the property to decrease the losses coming from the p-doped region. In particular, due to their refractive index, they make thicker the part of the waveguide around the active

region, that without SCH layers turns to be too thin in order to well confine the mode.

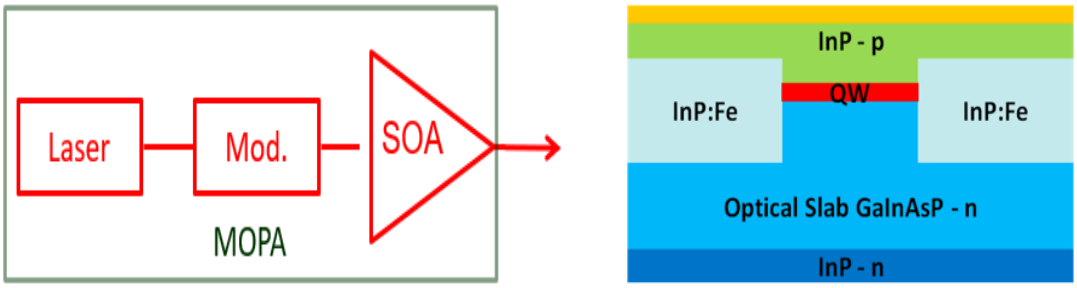

(a) (b)

Figure 2.1: MOPA optical circuit schematics (2.1a), and structure of the SCOW structure (2.1b)

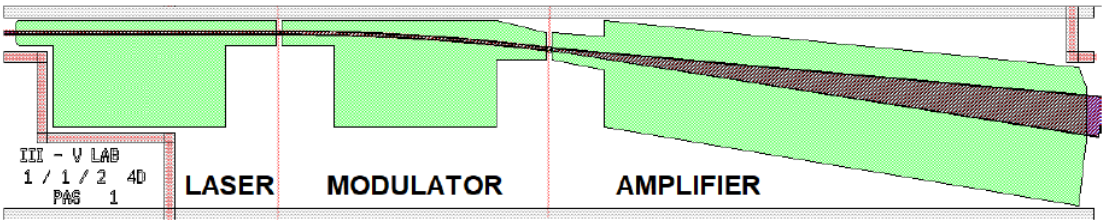

Figure 2.2: MOPA schematics

Chapter 3

Results

3.1 Simulation of the waveguide

In the following, simulations are carried out making use of the software ALCOR (described in details in the appendix) in order to study the guided mode inside the device, trying to increase its confinement in the active region, decreasing its propagation in the lossy p-doped layers, while keeping a monomode optical waveguide.
In order to quantify optical losses in the device, that are the main causes related to a low output power, the gain region of the device can be modelled as a directly biased PIN junction, in which carriers recombine in the intrinsic region. The active part of the device is thus divided into:

- the intrinsic part, concerning the active region and and the Separate Confinement Heterostructure (SCH) layers; its more important loss process is the re-absorption of photons in the quantum wells;
- the n-doped layer, that considers the n-doped InP substrate and the optical slab (massive or diluted), in which the main losses come from Free Carrier Absorption in the conduction band; in general these losses are lower compared to the other layers;
- the p-doped part, that considers the contacts and the p-doped InP layers. Here, at $1.55\,\mu m$, losses come mainly from the absorption of photons that promote electrons from the split-off to the valence band, because of the so-called 'Inter Valence Band Absorption' (IVBA) process. This latter is also the main loss component in the device, and for this reason, the guided mode is prevented to propagate in this section in order to reduce the overall losses, that in turn are important in order to maximize the output saturation power $P_{out,sat}$.

To improve the attraction of the propagating mode to the lower cladding, the simple n-doped slab (called the 'massive' slab) can be substituted by a more complex periodical structure known as the 'diluted' slab. This is mainly due to the fact that is technologically demanding to have a new alloy with a precise intermediate index; to overcome this issue the concept of effective refractive index is exploited, thanks to two already employable materials that can fulfill the refractive index requirement. The new kind of slab is thus a succession of different layers of two different materials with similar refractive indexes; for two materials with refractive indexes n_1 and n_2 and with thicknesses e_1 and e_2 the effective refractive index is defined as:

$$n_{eff} = \frac{n_1 e_1 + n_2 e_2}{e_1 + e_2} \tag{3.1}$$

the mode will thus be attracted by the effective refractive index, reducing losses in the p-doped region. The quantity which is used to calculate the overlap of the mode with

respect to a particular section of the waveguide is the confinement factor Γ, that can be expressed in percentage, and turns out to be important in the evaluation of the output saturation power [10]:

$$P_{out,sat} = \frac{dw}{\Gamma} \frac{\hbar\omega_0}{a_N \tau_c} \tag{3.2}$$

where $a_N = \partial g / \partial N$ the differential gain, d and w are the geometrical parameters of the active region $\hbar\omega_0$ is the photon energy and τ_c is the carrier lifetime. $P_{out,sat}$ has to be maximized, in order to shift the saturation of the power at a higher value, enabling an higher amplification [7] for the device. The confinement factor appears to be inversely proportional to the saturation power; an higher saturation power will be given by a lower Γ. The same parameter turns out to be directly proportional the material gain of the device:

$$g(N) = \Gamma a_N (N - N_{tr}) \tag{3.3}$$

where N_{tr} is the carrier density at transparency; thus, increasing the confinement over the active region, an higher material gain (related to an higher device gain) is then obtained.

3.1.1 Massive Slab architecture - Displacing the InP:Fe layer

Considering the massive slab structure, an analysis is performed on the effect of the InP:Fe barrier shift on the waveguide mode (3.1a,3.1b); this increases the confinement in the active region going up to $\Gamma_{AR} = 4.73\%$ (3.1a) and $\Gamma_{AR} = 4.82\%$ (3.1b); at the same time however the p-doped layer confinement increases up to $\Gamma_p = 11.04\%$ (3.1a) and $\Gamma_p = 11.23\%$ (3.1b). The advantage of this kind of structure, that includes both the index guiding and the horizontal guiding given by the SIBH structure, gives a more circular propagating mode, that can be better collected by outer systems.

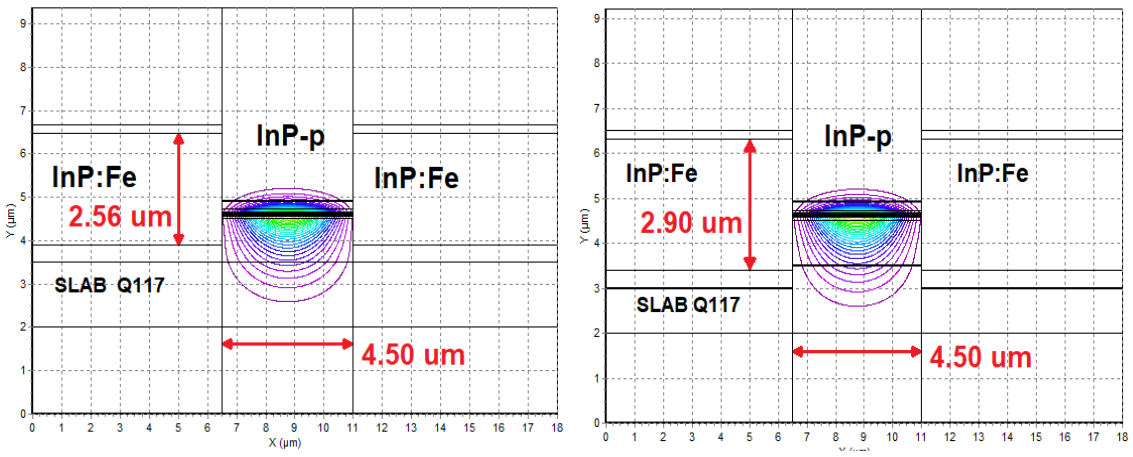

(a) 2.66 μm InP:Fe regrowth thickness

(b) 2.9 μm InP:Fe regrowth thickness

Figure 3.1: Simulated optical mode with massive slab structure

3.1.2 Massive Slab architecture - Reducing the thickness of the SCH layer

A second analysis for the massive slab architecture evaluates the impact of the SCH layer thickness variation; two kinds of studies are carried out, considering the symmetrical variation of the two layers thicknesses and the asymmetrical one. In the first case (3.2a), starting with the two SCH layers 30 nm-thick, that lead to a confinement in the active region of 3.14% and for the p-doped region 8.45%, reducing the thickness of both layers up to 10 nm, a decrease is seen in the two regions, the lower one being in the p-doped region. The drawback is however the decrease of confinement also in the active region.
The thickness variation is then considered asymmetrically in the two layers (3.2b): considering a structure with a low SCH layer 10 nm-thick and an high SCH layer 30 nm-thick, that shows $\Gamma_{AR} = 2.48\%$ and $\Gamma_p = 7.26\%$, an increase is obtained for the active region, but also for the p-doped one. To increase the confinement over the active region the opposite configuration (low layer 30 nm and high layer 10 nm) is simulated, leading to a very slight increase of Γ_{AR}, but having almost no increase for Γ_p. An increase of almost one unit arises in the case the low layer is 60 nm and the high layer is 30 nm; together with that, a big increase is seen for the p-doped layer ($\Gamma_p = 10.08\%$). The opposite situation has slightly better results with an increase for the active region with $\Gamma_{AR} = 4.16\%$ and a slight decrease for the lossy region, $\Gamma_p = 9.97\%$.

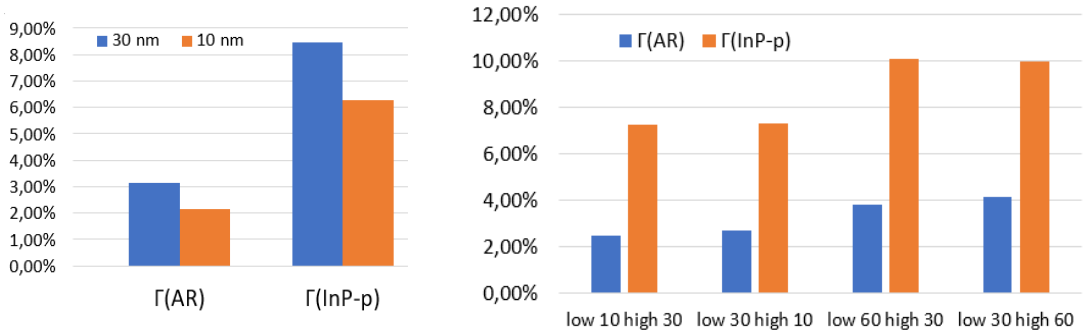

(a) Symmetric variation

(b) Asymmetric variation

Figure 3.2: Thickness variation of SCH layers

3.1.3 Diluted Slab architecture

Considering the SCOW structure with diluted slab architecture, with fifteen periods of layers of n-doped InP and layers of Q1.17, having an effective index $n_{eff} = 3.241$ and in the lower part of the slab (the first eight periods) $n_{eff} = 3.245$, the first simulation (3.3a) shows $\Gamma_{AR} = 3.45\%$ of confinement for the active region, and $\Gamma_p = 8.12\%$ in the p-doped region. Firstly, to have a larger output power, the active area has to be increased; this is obtained by increasing the width of the waveguide, that in the following cases is almost doubled. The other possibility that gives an higher output power is then to change the effective refractive index of the diluted slab, varying the thicknesses of the different layers. This enables the possibility to have a 'non uniform' diluted slab, in which slight

differences of effective refractive index are present. The first situation sees an higher n_{eff} in the lower part than in the upper. In (3.3b) the confinement in p-doped region is almost halved ($\Gamma_p = 4.99\%$), although a decrease is also present in the active region by one unit ($\Gamma_{AR} = 2.21\%$); the mode starts to be delocalized in the lateral part of the device with respect to the starting simulation, an important fraction of the mode is going down in the slab. Here the refractive index is varied by considering the first lower eight periods with $n_{eff} = 3.245$ and the remaining seven periods $n_{eff} = 3.250$; the structure is therefore the opposite of the starting one, having a lower part with a lower refractive index. Better

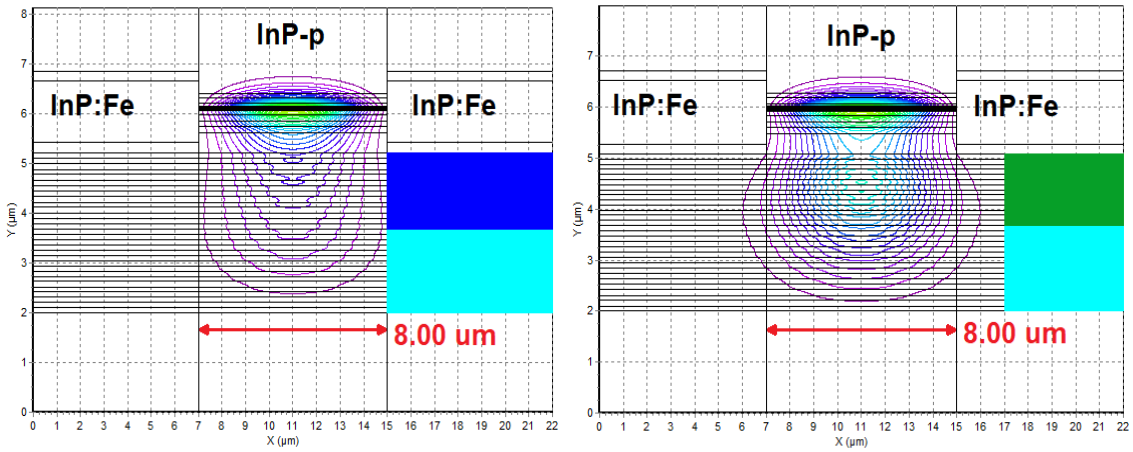

(a) Light blue part $n_{eff} = 3.245$, blue part $n_{eff} = 3.241$

(b) Light blue part $n_{eff} = 3.245$, dark green part $n_{eff} = 3.250$

Figure 3.3: Diluted slab structure: starting simulation (3.3a, inverted structure (3.3b)

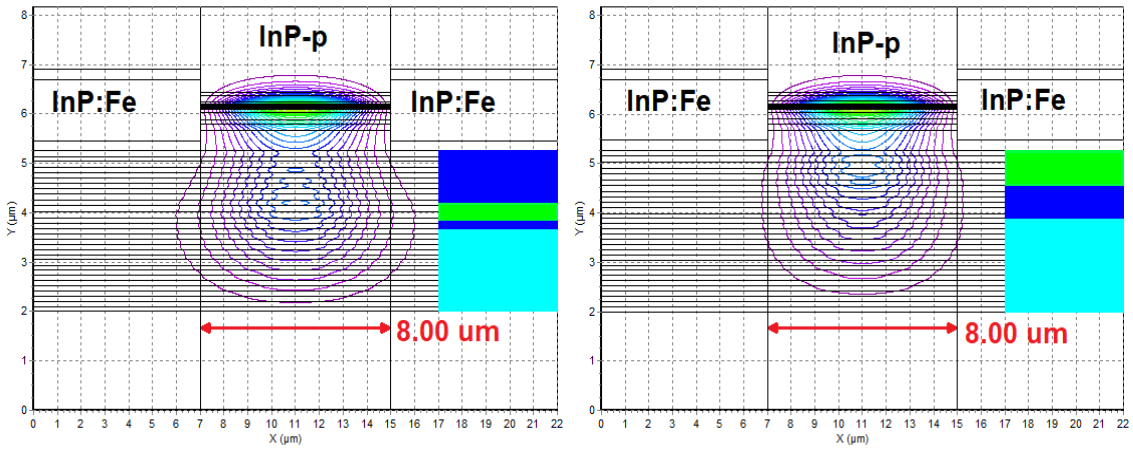

(a) Two periods introduced

(b) Three periods introduced

Figure 3.4: Introducing two and three periods of higher refractive index: light green part $n_{eff} = 3.249$, light blue part $n_{eff} = 3.245$, blue part $n_{eff} = 3.241$

values are then obtained in the following simulations (3.4a, 3.4b and 3.5), increasing of

only one unit the p-doped region confinement (5.79%,6.43% and 5.53% respectively), but maintaining to a value of almost 2.5% the active region contribution. The slab in 3.4a has a refractive index decreasing from bottom to top, with in the upper part two periods with the highest value, in order to attract more the mode in the upper part of the slab, in order to increase the confinement in the active region and to less deconfine the mode in the lateral part of the waveguide.
The following structure 3.4b sees the same structure as the previous one, but with this time the highest refractive index periods in the upper part of the slab; this has a good effect on the mode shape, concentrating it more in the center of the waveguide.
In simulation 3.5 instead, the extreme layers of the slab show the highest values of n_{eff}, with a low refractive index region in the center; the mode is more displaced, but better values are obtained for the confinement factor.
Summarizing, if a bigger refractive index region in the higher part of the slab is considered,

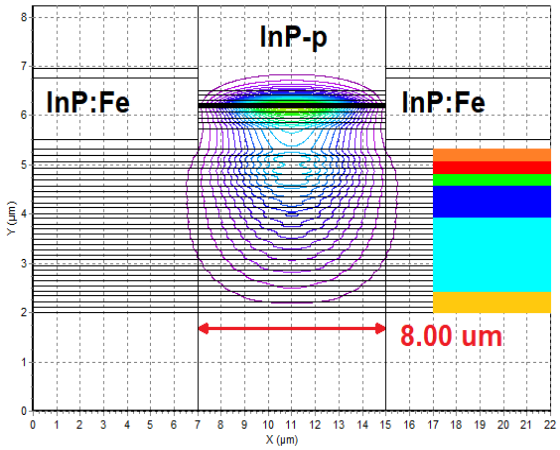

Figure 3.5: Highest refractive index part at the top and at the bottom: yellow $n_{eff} = 3.256$ (2 periods), light blue $n_{eff} = 3.245$ (7 periods), blue $n_{eff} = 3.241$ (3 periods), light green $n_{eff} = 3.249$ (1 period), red $n_{eff} = 3.252$ (1 period), orange $n_{eff} = 3.255$ (1 period)

good results are achieved in order to decrease losses; this has however a drawback because of the reduction to a low value of the active region confinement. A compromise can be obtained by considering the higher part of the slab with a low index, in which some periods of very high refractive index are added. This increases slightly the lossy region confinement, and at the same time increases the active region one (it maintains a value of 2.5% almost). A better compromise is then achieved when a high n_{eff} region is considered in the lowest periods of the slab; this leads to a $\Gamma_p = 5.53\%$.

3.2 Semiconductor Optical Amplifiers

The following section about the Semiconductor Optical Amplifier stage will be the base of a dynamical model that studies the impact of optical nonlinearities in gain and phase dynamics and on power and gain dependence along the length of the device.
Semiconductor Optical Amplifiers are directly derived from semiconductor lasers, but

differently from them they do not include an optical feedback. As in semiconductor lasers, the gain is created by the recombination of injected carriers from conduction to valence band. In an SOA, an input optical beam experiences amplification passing inside the device; this happens through stimulated emission. Denoting by z the propagation direction of the optical beam, the propagation of the electromagnetic field inside the amplifier is described by the wave equation ([1]):

$$\nabla^2 E - \frac{\epsilon}{c^2}\frac{\partial^2 E}{\partial t^2} = 0 \tag{3.4}$$

in which the dielectric constant ϵ describes both the dielectric waveguiding in the semiconductor medium (due to the difference of refractive indices) and the effect of injected carriers: $\epsilon = n_b^2 + \chi(N)$. Assuming a single propagating optical mode in the transverse directions x and y linearly polarized, the propagating optical field can be written as:

$$E(x,y,z,t) = \hat{\epsilon}\frac{1}{2}(\Phi(x,y)A(z,t)e^{(i(k_0 z-\omega_0 t))} + \Phi^*(x,y)A^*(z,t)e^{(-i(k_0 z-\omega_0 t))}) \tag{3.5}$$

where $\hat{\epsilon}$ is the polarization vector. Substituting this expression into the wave equation and considering only $A(z,t)$ ([1]), an equation is obtained for the evolution of the z-component, in which, describing $A(z,t)$ through the instantaneous power and phase $P(z,t)$ and $\phi(z,t)$, $A(z,t) = \sqrt{P}e^{i\phi}$, two equations are obtained for the variation of the power and phase of the beam along the length of the amplifier (considering no losses):

$$\frac{\partial P(z,t)}{\partial z} = g(z,t)P \tag{3.6}$$

$$\frac{\partial \phi(z,t)}{\partial z} = -\frac{1}{2}\alpha g(z,t) \tag{3.7}$$

The first one is the so-called 'Amplifier Equation', and $g(z,t)$ is the semiconductor material gain. 3.7 instead describes the phase evolution of the beam along the amplifier; this is directly proportional to the material gain through the linewidth enhancement factor α for the considered process.

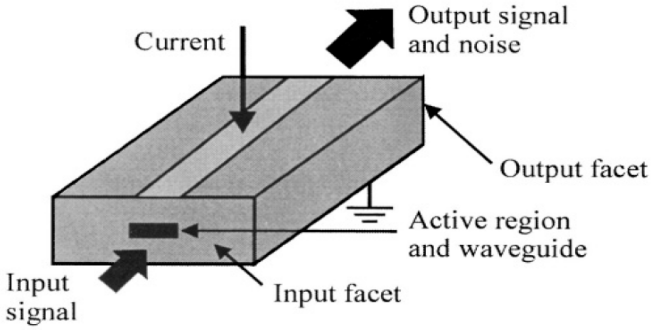

Figure 3.6: SOA schematics

3.3 Optical nonlinearities in semiconductors

Optical nonlinearities in SOAs are evaluated experimentally by performing a pump-probe experiment, in which a pulsed pump and a continous wave probe optical signals are sent inside the semiconductive waveguide, affecting the material gain. The material gain variation due to the picosecond pulse inside the amplifier leads to a variation for the refractive index through the so-called linewidth enhancement factor, or Henry's α-factor. This latter has the property of simplifying the well-known Kramers-Krönig relations. Material gain and refractive index changes are in turn related to the magnitude and phase of the beam propagating in the amplifier, that due to these effects will be not only affected by the gain coming from stimulated emission. According to [6] the following nonlinearities are present in semiconductor materials:

- Band Filling ('BF'): it is related to the overall population of carriers in the bands of the semiconductor; it is the succession of carrier depletion and carrier recovery effects. Carrier depletion ('CD') is a fast effect, because stimulated recombination is almost instantaneous on the timescale of the pulse duration; it also increases the refractive index of the material. Carrier recovery ('CR') is instead the refilling of electrons and holes to back to the concentration of the small signal gain, and has a characteristic timescale in the order of magnitude of hundreds of picoseconds.

- Carrier Heating ('CH'): it is a rapid process coming from the fact that picosecond pulses destroy the carrier equilibrium inside the band of the semiconductor material, and the instantaneous carrier occupation probability cannot be described anymore by a Fermi function; after the refill of carriers inside the band, carriers can be described this time by an effective Fermi function at a 'hot' carrier temperature. This process leads to a decrease in gain and an increase in refractive index of the material.

- Two Photon Absorption ('TPA'): is the simultaneous absorption of two photons with the same or different energies that together have the same energy as the material energy gap. Due to the very low probability to have the simultaneous absorption, effects related to TPA occur only at very high input powers. It is possible to discriminate from 'degenerate' TPA when the two photons come from the same input signal, and to 'nondegenerate TPA' when the two photons come from two different input signals.

- Free Carrier Absorption induced by TPA ('FCA'): carriers that are promoted to the conduction band by two photon absorption can become available for free carrier absorption. In general absorption promotes carriers to the valley in the first Brillouin zone center (the so-called Γ-valley); if this latter is already filled, or the total energy for the two photons is very high, due to the presence of a phonon, the neighbour X-valley can be filled. Carriers in X-valley can be then promoted to an higher conduction band (which is nearer to X-valley than to the Γ-valley) by means of the absorption of a photon that enables a direct transition to a upper band.

One nonlinear effect which will not be considered in the analysis is Spectral Hole Burning ('SHB'), which is linked to carrier depletion by the pump signal; the change in gain has a symmetric spectral profile around the frequency of the pump, giving no changes to the refractive index. Also the probe contribution to refractive index is not considered, because

pump and probe frequencies are approximately the same. In particular the following model will not consider also gain changes induced by SHB, because these latter are almost negligible in the SOAs available in the laboratory.
Nonlinear phenomena are modeled in the expression of the material gain by the introduction of gain compression factors. These latter are derived from density matrix equations in the relaxation time approximation ([2],[5]), that lead to rate equations, for both the instantaneous carrier density and carrier energy; introducing phenomenological terms into these latter, accounting for nonlinear processes, they lead to phenomenological constants (the gain compression factors), that can be derived from experiments and that take into account the departure from the linear behaviour for the material gain.
The introduction of carrier heating in the material gain consists in dividing the small signal gain by a term containing the product of the CH gain compression factor and the power propagating into the device; the TPA process is instead phenomenologically inserted in the numerator:

$$g(N) = \frac{g_0 - \epsilon_{TPA} P^2}{1 + \epsilon_{CH} P} \tag{3.8}$$

the TPA term is proportional to the square of the power passing through the SOA (due to the double-photon nature of the process).
Band Filling is also added phenomenologically, relating it to the carrier density inside the amplifier as $\Delta g_{BF} = \Gamma a_N (N - N_{st})$, where $N_{st} = I\tau_c/eV$ represents the unsaturated value of the carrier density. This contribution is added to the small signal gain and adding carrier heating to the model, solving for the material gain $g(N)$:

$$g(N) = \frac{g_0 - \epsilon_{TPA} P^2 + \Delta g_{BF}}{1 + \epsilon_{CH} P} \tag{3.9}$$

The TPA contribution is introduced in the numerator of the expression, and having that the small signal gain can be written as: $g_0 = \Gamma a_N (N_{st} - N_{tr})$, where N_{tr} is the carrier density at transparency. Substituting in the previous expression:

$$g(N) = \frac{\Gamma a_N (N - N_{tr}) - \epsilon_{TPA} P^2}{1 + \epsilon_{CH} P} \tag{3.10}$$

in which the linear dependence of the gain with respect to carrier density is shown.

3.4 Optical nonlinearities modeling in the SOA stage

In the following, a numerical model is presented, in order to analyze the impact of optical nonlinearities in the SOA; nonlinearities will be the key effects in order to perform amplitude and phase modulation in the SOA. The following model mainly follows the article by Marculescu et al. ([6]). In order to characterize nonlinear effects in the device, a pump-probe experiment is performed, studying gain and refractive index dynamics, by introducing a strong picosecond pump pulse and a weak continous wave probe signal. In order to simplify the analysis, some assumptions are considered:

- the SOA waveguide is single-mode propagative;

- the mode is assumed to be a plane wave with effective propagation constant $k_0 n_0$ and effective refractive index n_0;
- the probe light power P_X is assumed to be much smaller than pump light power P_S, so there is no phase relation between the two signals;
- the frequency of the two signals is almost the same $\omega_S \approx \omega_X \approx \omega_0$;
- both signals propagate with the same group velocity v_g, and have a negligible group velocity dispersion;
- the pump power will influence the amplification and phase shift for both pump and probe light, so all processes will be treated as if they happened in the absence of the probe;
- device's losses are neglected in the model ($\alpha_{int} = 0$).

The first analysis consists in the study of material gain and refractive index dynamics deriving from the propagation of the picosecond pump pulse inside the amplifier; this latter impacts on the carrier density of the semiconductor in the amplifier, that in turn affects the material gain and refractive index. Gain and index variations with respect to carrier density are related by the linewidth enhancement factor, or Henry α-factor:

$$\alpha_N = -2k_0 \frac{\partial n/\partial N}{\partial g/\partial N} \approx -2k_0 \frac{\Delta n}{\Delta g} \tag{3.11}$$

in this case, the parameter is defined in particular for the carrier density N, but it can be defined in general for every quantity (see [2]).
The dynamics of the material gain can be directly obtained starting from the rate equation for the carrier density inside the amplifier that, due to amplification of a pulse, is considered in the retarded time frame $\tau = t - z/v_g$:

$$\frac{\partial N}{\partial \tau} = \frac{I}{eV} - \frac{N}{\tau_c} - \frac{g(N)P}{\hbar\omega_0 \sigma_m} \tag{3.12}$$

in which the first term is related to current pumping, the second term to recombination processes (with characteristic recombination time τ_c), and the latter to the loss of carriers due to stimulated emission. This term is chosen in the equation for simplicity to be proportional to the power of the incoming beam P rather than to the photon density S; the two quantities are related by $P = \hbar\omega_0 \sigma_m v_g S$ where $\hbar\omega_0$ is the photon energy, σ_m the active region area and v_g the group velocity. Making the assumption of a linear dependence of the material gain on the carrier density, $g(N(\tau)) = \Gamma a_N (N(\tau) - N_{tr})$, and noting that: $\frac{\partial N}{\partial \tau} = (1/\Gamma a_N)(\partial g/\partial \tau)$, the following relation for the time evolution of the material gain is derived in the retarded time frame:

$$\frac{\partial g}{\partial \tau} = -\frac{g - g_0}{\tau_c} - \frac{gP}{E_s} \tag{3.13}$$

Where P_s is the saturation power of the amplifier and $E_s = P_s \tau_c$ is the saturation energy; defining the unperturbed small signal gain as $g_0 = \Gamma a_N (I\tau_c/eV - N_{tr})$. In order to relate

the gain dynamics to the shape of the input pump pulse, the integrated gain, that will be useful throughout the model, is introduced, by integrating the amplifier equation along the length of the SOA:

$$h(\tau) = \int_0^L g(z,\tau)dz \tag{3.14}$$

this leads to a simple expression for the device amplification:

$$P_{out}(\tau) = P_{in}(\tau)e^{h(\tau)} = G(\tau)P_{in}(\tau) \tag{3.15}$$

in which the input pulse is directly related to the output pulse by means of the device gain $G(\tau) = e^{h(\tau)}$. Introducing the same concept in equation (3.13), and denoting as the small signal integrated gain the quantity $h_0 = g_0 L$, the following differential equation is obtained, describing the time evolution of the integrated material gain depending on the input pulse inside the amplifier [4]:

$$\frac{dh}{d\tau} = \frac{h_0 - h}{\tau_c} - \frac{P_{in}(\tau)}{E_s}(e^h - 1) \tag{3.16}$$

in which a gaussian input pulse is considered as $P_{in}(\tau)$ for the amplifier. Equation (3.16) is then solved numerically through a finite difference technique (later explained in the appendix), considering as initial condition $h(\tau = 0) = h_0$ (which is the gain of the device before the arrival of the pulse). From this, the device gain $G(\tau)$ is derived, together with the output pulse shape $P_{out}(\tau) = G(\tau)P_{in}(\tau)$.
Together with that, the phase variation in time is derived, having previously integrated the phase equation along the length of the device (3.7):

$$\phi_{out}(\tau) - \phi_{in}(\tau) = -\frac{1}{2}\alpha_N h(\tau) \tag{3.17}$$

the previously described nonlinear effects are inserted in the model, in order to obtain the material gain and refractive index dynamics that derive from the propagation of a picosecond pulse inside the amplifier. For what concerns the gain dynamics, this is directly related to the integrated gain counterpart; the main point of the analysis is to calculate, for each nonlinear effect i, the related change in the integrated gain $\Delta h_i(\tau)$ and summing it to the unperturbed (linear) one, $h(\tau) = h_0 + \sum_i \Delta h_i(\tau)$. The first effect analyzed is band filling; considering a pump-probe experiment with a negligible probe light, and the gain being only varied by the band filling effect, i.e. $g(z,\tau) = g_0 + \Delta g_{BF}$, substituting this expression in (3.13) the following equation is derived:

$$\frac{\partial \Delta g_{BF}}{\partial \tau} = -\frac{gP}{E_s} - \frac{\Delta g_{BF}}{\tau_c} \tag{3.18}$$

that expresses the dynamics of the material gain variation for the band filling contribution. Having that the unsaturated gain coefficient is always larger than the band filling gain coefficient, it turns out that $\Delta g_{BF} < 0$. The first term in the right hand side is thus negative and accounts for the power gain decrease induced by carrier depletion ; the second term is instead positive, and accounts for an increase in the gain in a time scale of τ_c, describing carrier recovery. Due to the excitation by the picosecond pulse, depletion and recovery occur on different time scales, giving the possibility to treat separately the two

effects. Depletion is almost instantaneous (occurs in a shorter time scale) with respect to recovery, that is in the order of magnitude of τ_c. Due to this, it is possible to separate the two contributions in the equation. In the limit of only carrier depletion 3.18 becomes:

$$\frac{\partial \Delta g_{CD}}{\partial \tau} = -\frac{(g_0 + \Delta g_{CD})P}{E_s} \tag{3.19}$$

to obtain an equation for the integrated gain, that is directly related to the given input pulse, equation (3.19) is integrated along the length of the SOA:

$$\frac{\partial \Delta h_{CD}}{\partial \tau} = -\frac{(e^{h_0+\Delta h_{CD}} - 1)}{E_s} P_{in} \tag{3.20}$$

the equation is then solved with the initial condition $\Delta h_{CD}(-\infty) = 0$ (i.e.: there is no effect of depletion at the beginning) leading to the following expression:

$$\Delta h_{CD} = -ln\left(e^{h_0} - (e^{h_0} - 1)exp\left(-\frac{1}{E_s}\int_{-\infty}^{\tau} P_{in} d\tau'\right)\right); \tag{3.21}$$

in which, considering a Gaussian input pulse, the integral of the input power is given in term of the error function [4]. Carrier depletion is considered effective up to a time $-\tau_r$ which is the beginning of gain saturation. This latter can be determined (a method to obtain it is present in [6] appendix) numerically and experimentally. After this time, carrier recovery is the leading phenomenon.
Considering the limit of only carrier recovery in 3.18:

$$\frac{\partial \Delta g_{CR}}{\partial \tau} = -\frac{\Delta g_{CR}}{\tau_c} \tag{3.22}$$

this expression simply leads to the equation for the integrated gain, that is solved considering as initial condition $\Delta h_{CR}(\tau_R) = \Delta h_{CD}(\tau_R)$. This gives the following expression for $\tau > \tau_R$:

$$\Delta h_{CR}(\tau > \tau_R) = \Delta h_{CD}(\tau_R) exp\left(-\frac{\tau - \tau_R}{\tau_c}\right) \tag{3.23}$$

summarizing, the band filling contribution is the succession depletion and recovery, separated by the characteristic time τ_R:

$$\Delta h_{\mathrm{BF}}(\tau) = \begin{cases} \Delta h_{\mathrm{CD}}(\tau) & \tau \leq \tau_{\mathrm{R}} \\ \Delta h_{\mathrm{CD}}(\tau_{\mathrm{R}}) \exp\left(-\frac{\tau-\tau_{\mathrm{R}}}{\tau_s}\right) & \tau > \tau_{\mathrm{R}} \end{cases} \tag{3.24}$$

the band filling contribution is then summed to the unperturbed integrated gain, in order to have the integrated gain with only the effect of band filling and then is inserted in the SOA gain, to account for the gain dynamics perturbed by the effect $G_{BF}(\tau) = e^{h_{BF}(\tau)}$.
To introduce carrier heating phenomena, starting from the contribution given by Δg_{CH} [6]:

$$\Delta g_{CH}(z,\tau) = -\epsilon_{CH} g(z,\tau) P = -\epsilon_{CH} \frac{(g_0 + \Delta g_{BF})P}{1 + \epsilon_{CH} P} \tag{3.25}$$

substituting the gain comprising both carrier heating and band filling effects, due to the fact that the model has to take into account both phenomena at the same time, the expression

on the r.h.s. is obtained. The effect of carrier heating occurs simultaneously with carrier depletion, implying that $g(z,\tau) = g_0 + \Delta g_{CD}$. Substituting in the expression the amplifier equation:

$$\Delta g_{CH} = -\frac{d}{dz}(ln(1+\epsilon_{CH}P)) \tag{3.26}$$

integrating this expression, the related change in the integrated gain is obtained:

$$\Delta h_{CH} = -ln\left(\frac{1+\epsilon_{CH}P_{in}(\tau)e^{h_0+\Delta h_{CD}}}{1+\epsilon_{CH}P_{in}(\tau)}\right) \tag{3.27}$$

in which the boundary conditions $P(0,\tau) = P_{in}$ and $P(L,\tau) = P_{in}e^{h_0+\Delta h_{CD}}$ were considered; due to the fact that CH occurs simultaneously with CD, only this part of band filling is considered ([6]). As in the previous case, the overall integrated gain is calculated starting from the previous band filling-dependent expression, and this latter takes part of the carrier heating dependent device gain.
Then two photon absorption is analyzed; in the limit of only degenerate processes, the gain variation (which is gain reducing) due to two photon absorption is given by:

$$\Delta g_{TPA} = -\frac{\beta_2}{A_{TPA}}P \tag{3.28}$$

where β_2 is the TPA absorption coefficient, that depends on pump frequency, and A_{TPA} is the effective TPA cross section, that includes also layers of the waveguide cladding; on this area the confinement factor for the TPA process Γ_2 is defined (later introduced in 3.37). To obtain the related change in the integrated gain, in this case the integral of the power along the SOA has to be performed; this can be solved (as in the appendix of [6]) by the use of derived coefficients, that enable the possibility to have an expression directly related to the input power:

$$\Delta h_{TPA}(\tau) = -\epsilon_{TPA}(e^{h_0}-1)C_1P_{in} \tag{3.29}$$

with the coefficient C_1 being equal to $C_1 = |\Delta h_{CD}|/(e^{|\Delta h_{CD}|}-1)$.
This contribution is added to the previous ones to obtain the overall effect on the integrated gain and on the related device gain. In the case of non-degenerate processes, in order to account also for the probe light, following the derivation of [6], the variation due to pump light remains the same and is taken to be the already derived quantity $\Delta h_{TPA,S}(\tau) = \Delta h_{TPA}(\tau)$, while for the probe light the TPA non-degeneracy factor r_{TPA} is introduced, giving the possibility to describe the contribution coming from the probe to be dependent on the degenerate variation:

$$\Delta h_{TPA,X}(\tau) = r_{TPA}\Delta h_{TPA}(\tau) \tag{3.30}$$

therefore, an 'effective' non-degenerate TPA-induced change $\Delta h_{TPA,tot}$ can be defined as the sum of the two contributions from the two signals. An evaluation of the integrated gain and of the device gain is performed introducing non-degenerate TPA by only substituting the latter expression at the place of Δh_{TPA}.
Following the same pattern, the phase variation induced by nonlinearities in the integrated gain dynamics is calculated; for each non linear process, the related linewidth enhancement factor is employed; starting from the first (linear) contribution:

$$\Delta\phi(\tau) = -\frac{1}{2}\alpha_N h(\tau) \tag{3.31}$$

the following pattern is employed for the induced phase variations:

$$\Delta\phi_x(\tau) = -\frac{1}{2}\alpha_x h_x(\tau) \tag{3.32}$$

with $x = \{BF, CH, TPA\}$. In this way the previously obtained quantities Δh_x can give the related nonlinear change in phase, that is summed to the already calculated phase.

$$\Delta\phi_{tot}(\tau) = -\sum_x \frac{1}{2}\alpha_x h_x(\tau) \tag{3.33}$$

The analysis of phase dynamics considers the modelling of free carrier absorption (FCA) induced by TPA, following [6], in which a simple expression is obtained for $\Delta\phi_{FCA}$, mainly related on h_0 and on the input pulse power. The study of the phenomenon starts from the related index change, that is modeled in the framework of the classical oscillator model of Drude and Lorentz, assuming electrons moving due to Newton's law. Studying the dynamics of the photoexcited electrons with average lifetime τ_{ex} that arise in the active region by TPA coming from the pump signal, and studying the system at the steady state and for a weak probe light, the FCA-related change of the refractive index is obtained:

$$\Delta n_{FCA} = -\frac{c}{\omega_0} g_0 \eta_{FCA} \epsilon_{TPA} P^2(z, \tau - \tau_{0,FCA}) \tag{3.34}$$

where $\tau_{0,FCA}$ is the intervalley scattering time that describes the electron transit time from the Γ to the X valley of the semiconductor, and η_{FCA} is the nonlinear optical coefficient for the FCA process, which is measured in W^{-1}. The expression (3.34) will be also used in the refractive index dynamics analysis. In order to account for the contribution in the phase dynamics, the previous expression for the gain has to be integrated along the length of the device; the integration involves the input power, needing the use of coefficients previously used in the TPA analysis:

$$\Delta\phi_{FCA} = \eta_{FCA}\epsilon_{TPA}(e^{h_0} - 1)^2 C_2(\tau - \tau_{0,FCA}) P^2(\tau - \tau_{0,FCA}) \tag{3.35}$$

From the gain dynamics, the refractive index dynamics is simulated, starting from the different equations giving the time evolution of Δg_x where x is denoting the different nonlinearities. From the gain changes, the related index change is given by the Henry's factor proportionality. The analysis is performed both considering only degenerate TPA processes and also including nondegenerate processes.
What is then simulated is the influence of nonlinear effects in the carrier density, and after the influence of the 'perturbed' carrier density on the material gain. The analysis starts from equation 3.12 that is then varied, accounting for the different processes. Except from the unperturbed equation, the first effect to be inserted is carrier heating:

$$\frac{\partial N}{\partial \tau} = \frac{I}{eV} - \frac{N}{\tau_c} - \frac{\Gamma a_N (N - N_{tr})}{1 + \epsilon_{CH} P} \frac{P}{\hbar\omega_0 \sigma_m} \tag{3.36}$$

Two photon absorption is introduced following [3]:

$$\frac{\partial N}{\partial \tau} = \frac{I}{eV} - \frac{N}{\tau_c} - \frac{\Gamma a_N (N - N_{tr}) - \epsilon_{TPA} P^2}{1 + \epsilon_{CH} P} \frac{P}{\hbar\omega_0 \sigma_m} + \frac{\Gamma_2}{\Gamma}\beta_2 \frac{P^2}{(\hbar\omega_0\sigma_m)^2 v_g} \tag{3.37}$$

in which Γ_2 is the confinement factor for TPA process. Obtaining the carrier dynamics in the three different cases, this latter is then substituted into the material gain in the approximation of linear gain, in order to analyze the material gain dependence with carrier density.
The following part is instead related to the investigation of the behaviour of the material gain along the length of the amplifier, deriving an equation which is able to represent the variation of the gain along the z-direction, i.e. dg/dz. Before doing this, the power along z is investigated with all possible nonlinearities, through the amplifier equation. The previously obtained gain deriving from carrier density dynamics is inserted in the amplifier equation, starting from the non perturbed one (equation 3.6), considering step by step the different nonlinearities:

$$\frac{\partial P}{\partial z} = \frac{\Gamma a_N (N - N_{tr})}{1 + \epsilon_{CH} P} P \tag{3.38}$$

firstly including carrier heating and band filling, then TPA [3]:

$$\frac{\partial P}{\partial z} = \frac{\Gamma a_N (N - N_{tr}) - \epsilon_{TPA} P^2}{1 + \epsilon_{CH} P} P - 2\Gamma_2 \beta_2 \frac{1}{\sigma_m} P^2 \tag{3.39}$$

the proposed model evaluates the change of the material gain with respect to the z-direction in the device; in the simplest situation (without the presence of nonlinearities) the main idea is to derive one more time with respect to z the amplifier equation; from:

$$\frac{\partial P}{\partial z} = g(z, \tau) P \tag{3.40}$$

deriving the equation one more time with respect to the z direction:

$$\frac{\partial^2 P}{\partial z^2} = \frac{\partial g(z, \tau)}{\partial z} P + g(z, \tau) \frac{\partial P}{\partial z} \tag{3.41}$$

the variation of the material gain along the z direction can be obtained:

$$\frac{\partial g(z, \tau)}{\partial z} = \left(\frac{\partial^2 P}{\partial z^2} - g(z, \tau) \frac{\partial P}{\partial z} \right) \frac{1}{P} \tag{3.42}$$

the equation is then solved, and $g(z)$ is obtained along the amplifier.
Carrier heating is included:

$$\frac{\partial P}{\partial z} = \frac{g(z, \tau)}{1 + \epsilon_{CH} P} P \tag{3.43}$$

deriving the expression:

$$\frac{\partial^2 P}{\partial z^2} = \frac{\partial}{\partial z} \left(\frac{g(z, \tau)}{1 + \epsilon_{CH} P} \right) P + \left(\frac{g(z, \tau)}{1 + \epsilon_{CH} P} \right) \frac{\partial P}{\partial z} \tag{3.44}$$

the following equation is obtained:

$$\frac{\partial g(z, \tau)}{\partial z} = \left(\frac{\partial^2 P}{\partial z^2} - \frac{g(z, \tau) \epsilon_{CH} P}{1 + \epsilon_{CH} P} \frac{\partial P}{\partial z} - \frac{g(z, \tau)}{1 + \epsilon_{CH} P} \frac{\partial P}{\partial z} \right) \frac{1 + \epsilon_{CH} P}{P} \tag{3.45}$$

the last equation can be considered to be an extension of the first derived one, because for $\epsilon_{CH} = 0$, the first model is recovered. The same method is employed including two photon absorption:

$$\frac{\partial P}{\partial z} = \frac{g(z,\tau) - \epsilon_{TPA}P^2}{1 + \epsilon_{CH}P}P - 2\Gamma_2\beta_2\frac{P^2}{\sigma_m} \tag{3.46}$$

deriving:

$$\frac{\partial^2 P}{\partial z^2} = \frac{\partial}{\partial z}\left(\frac{g(z,\tau) - \epsilon_{TPA}P^2}{1 + \epsilon_{CH}P}\right)P + \left(\frac{g(z,\tau) - \epsilon_{TPA}P^2}{1 + \epsilon_{CH}P}\right)\frac{\partial P}{\partial z} - 2\Gamma_2\beta_2\frac{1}{\sigma_m}\frac{\partial P^2}{\partial z} \tag{3.47}$$

substituting into the previous equation and simplifying, solving for $\partial g/\partial z$:

$$\frac{\partial g}{\partial z} = \frac{1 + \epsilon_{CH}P}{P}\frac{\partial^2 P}{\partial z^2} + (\epsilon_{TPA}2P)\frac{\partial P}{\partial z} - \frac{g - \epsilon_{TPA}P^2}{1 + \epsilon_{CH}P}\epsilon_{CH}\frac{\partial P}{\partial z} - \frac{g - \epsilon_{TPA}P^2}{P}\frac{\partial P}{\partial z} + 4\Gamma_2\beta_2\frac{1 + \epsilon_{CH}P}{\sigma_m}\frac{\partial P}{\partial z} \tag{3.48}$$

also in this case, in the absence of effects ($\epsilon_{TPA} = \epsilon_{CH} = \beta_2 = 0$) the first derived expression is obtained. Note that for each of these derived expressions the band filling effect has been already encountered in the material gain: $g(z,\tau) = g_0 + \Delta g_{BF}$.

3.4.1 Numerical simulation

Following [6] and [8], an SOA with a length $L = 2.6\,mm$ is simulated, considering a gaussian input pulse of $3.8\,mW$ peak power with a FWHM of $2.8\,ps$ in the time interval $[-5\,ps, 10\,ps]$. An input pump current of $350\,mA$ is considered, together with a $\tau_c = 100\,ps$ and saturation power $P_{sat} = 50\,mW$. What turns out from the simulation is that the same results as [6] are obtained for a lower input pump current (the article considered a pump current of $I = 400\,mA$). The first simulated quantity is the integrated gain $h(\tau)$ without the presence of nonlinearities (3.7a), with the related device gain $G(\tau)$ (3.7b). What is obtained is a constant value of $h(\tau)$ and $G(\tau)$ as time increases (3.7a), the device amplifies with the same amount at each value of power. The output pulse without nonlinearities is then calculated

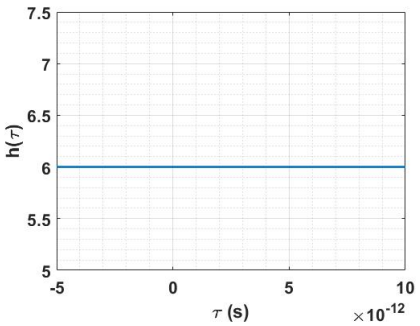

(a) Integrated gain dynamics

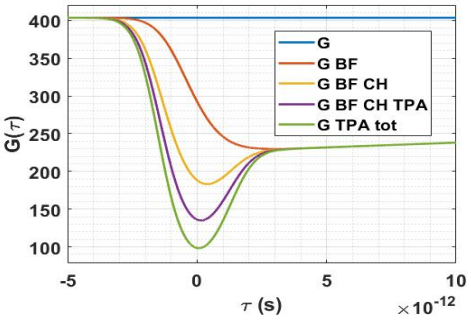

(b) Device Gain dynamics in presence of nonlinearities

Figure 3.7: Unperturbed $h(\tau)$; $G(\tau)$ in presence of nonlinearities

(3.8a,3.8b), showing the pulse amplification by the SOA.
The different effects are introduced in the integrated gain $h(\tau)$ (3.9a) and a good agreement

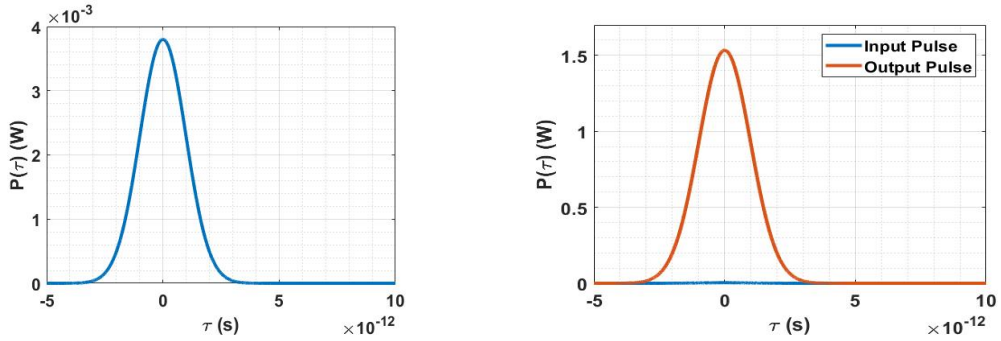

(a) Input pulse (b) Amplified output pulse

Figure 3.8: Input and output pulses

is noticed with respect to [6]; the integrated gain is thus decreasing adding each nonlinearity. Following [6] appendix, τ_R is determined to be 3.3 ps, treating separately carrier depletion and recovery. As in the reference, the different effects lead to a bigger decrease of the $h(\tau)$ together with the maximum of the input pulse. In the simulated data, also the integrated gain without nonlinearities (the blue curve in 3.9a) and the contribution of nondegenerate TPA are modeled (green curve in 3.9a).
The effect of nonlinearities is evaluated also in the output pulse (3.10a); the overall effect is firstly a decrease of the gain, leading to a weaker output pulse, and more asymmetric pulses, due to the fact that the two edges of the pulse experience different amplification ;this is due to the leading pulse edge that saturates the amplifier and decreases the gain of the device, directly related to the material gain [4] (as stated in [4]).
Then the phase variation of the beam is evaluated, firstly in absence of nonlinearities

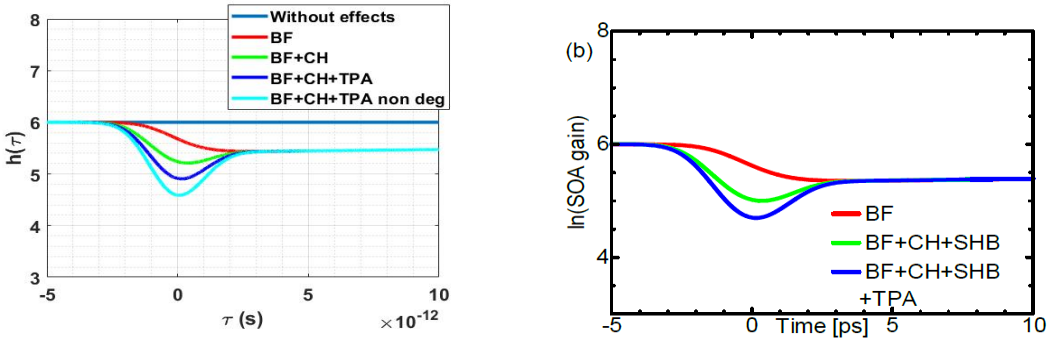

(a) Simulated integrated gain dynamics (unperturbed $h(\tau)$ and nondegenerate TPA added)

(b) From reference [6]

Figure 3.9: Integrated gain dynamics comparison taking into account nonlinearities

(3.10b); subsequently, nonlinearities are encountered (3.11a): noting that in 3.11b ordinates are inverted; a good agreement is present for all effects, remembering that in the simulation

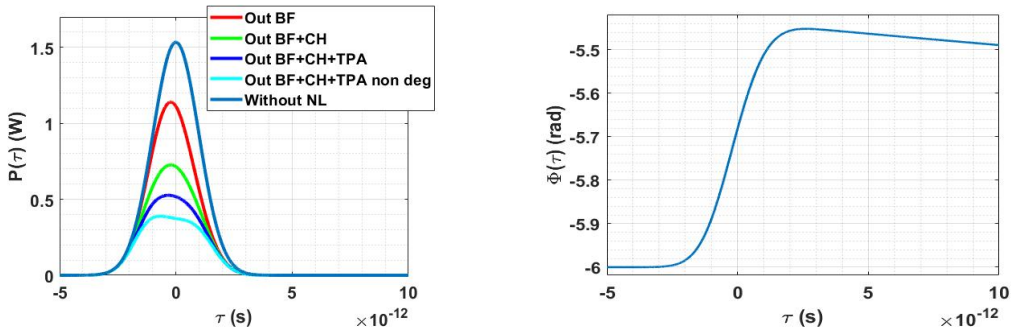

(a) Simulated output pulse with nonlinearities (b) Simulated phase dynamics

Figure 3.10: Output pulse in presence of nonlinearities - Unperturbed phase dynamics

a current of almost $350\,mA$ was considered; considering a current of $400\,mA$ instead, the simulation obtains a small signal integrated gain of almost $h_0 \approx 6.78$, which is higher than the $h_0 = 6$ considered in the paper. h_0 is in fact the quantity that affects the most the FCA contribution, changing the peak value of the phase shift.

Then, the refractive index dynamics is studied in presence of effects (3.12a); what is shown

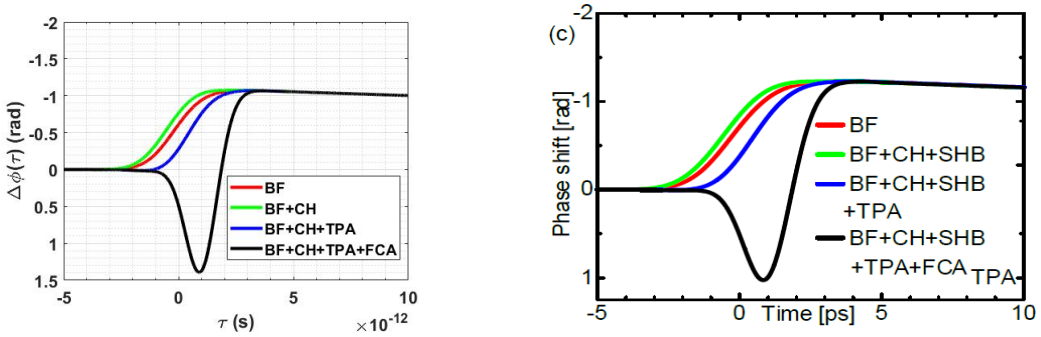

(a) Simulated phase dynamics (b) From reference [6]

Figure 3.11: Phase dynamics comparison in presence of nonlinearities

are the different Δn_x variations, as in the article; in the simulation also the unperturbed index dynamics is considered. Up to having considered TPA processes, the behaviour is in agreement to [6], but evaluating the free carrier absorption induced by TPA, the theoretical dip which is expected slightly above the pulse peak is not present, and the curve seems to follow the one with TPA contribution. This can be due to the timescale definition of the process (which is translated by the time required to reach the X-valley of the semiconductor), but also by the power squared-dependence of the process, that seems to have a very small contribution in the simulation, or to contribute badly in the article. The main source of discrepancies can be however the fact that SHB is not considered both in gain and in index dynamics (as previously assumed).

For what concerns the analysis of the carrier density in presence of nonlinearities, the obtained $N(\tau)$ (3.13a) has a decrease (that can be considered part of the carrier depletion

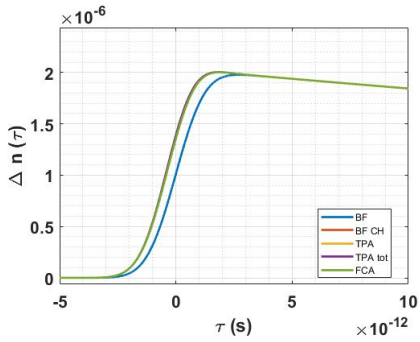

(a) Simulated refractive index dynamics (non degenerate TPA is added with respect to [6])

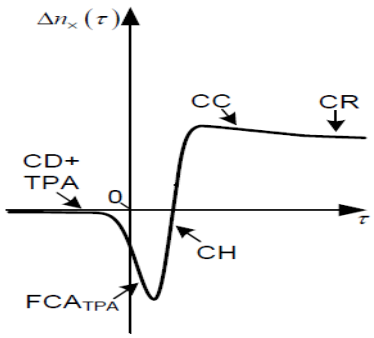

(b) From [6]

Figure 3.12: Refractive index dynamics comparison in presence of nonlinearities

phenomenon) during pulse amplification, and has a very slow increase (beginning of carrier recovery) after the pulse. Nonlinear effects are most evident especially during the recovery, in which some effects increase the speed of recovery, even if there are very slight departures from the unperturbed curve.
The material gain dependence with respect to carrier density (3.13b) is the well-known linear one (when only BF is considered); very slight departures from nonlinearities can be seen at low values for the carrier density. The material gain time dependence is then

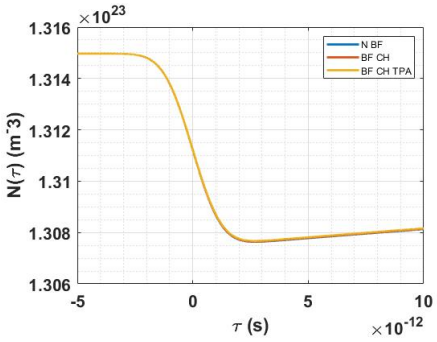

(a) Carrier density dynamics $N(\tau)$

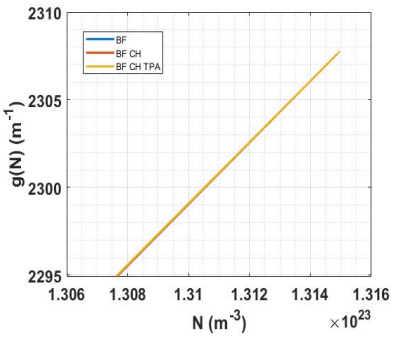

(b) Material gain dependence with carrier density

Figure 3.13: Simulated carrier density dynamics and related material gain

calculated, and follows the carrier density (3.14a); multiplying it by the length of the SOA the integrated gain is obtained (3.14b), that clearly follows $h(\tau)$ calculated before by the solution of equation (3.16). This shows the similarity of the two methods employed to obtain the integrated gain: by starting from the equation of the evolution of $h(\tau)$, or by solving the carrier density rate equation and obtaining the integrated gain by the material gain evolution. What gives in addition the second method is the evolution of the material gain, which is not given by the first method, that starts already from the integrated gain.
For the length-dependence of the power and the material gain all along the SOA (obtained in the derived model), due to CH and TPA, a lower value for both the gain (3.15b) and

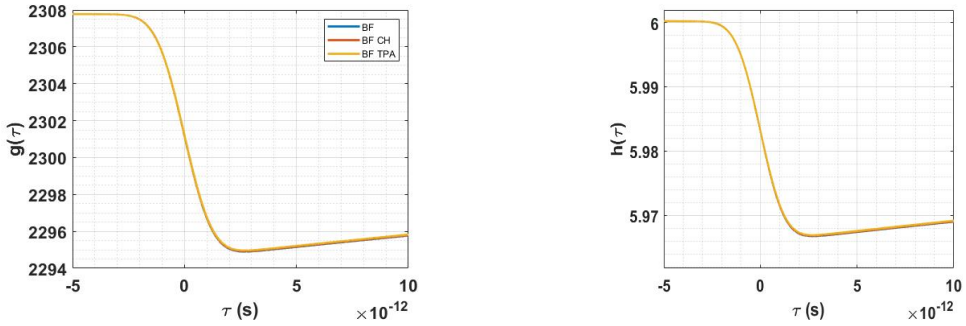

(a) Material gain $g(\tau)$ (b) Integrated gain $h(\tau)$

Figure 3.14: Simulated material gain and integrated gain dynamics derived from carrier density

power (3.15a) is reached. This comes from the fact that at each section along the length of the SOA the material gain is reduced because of nonlinearities and this leads to a lower amplification along the device, that then gives a lower power at the output section. Results are considered with the power at $\tau = 0\,ps$ (considering as the peak power of the pulse). The dependence of the device gain with the output pulse power is then investigated in the

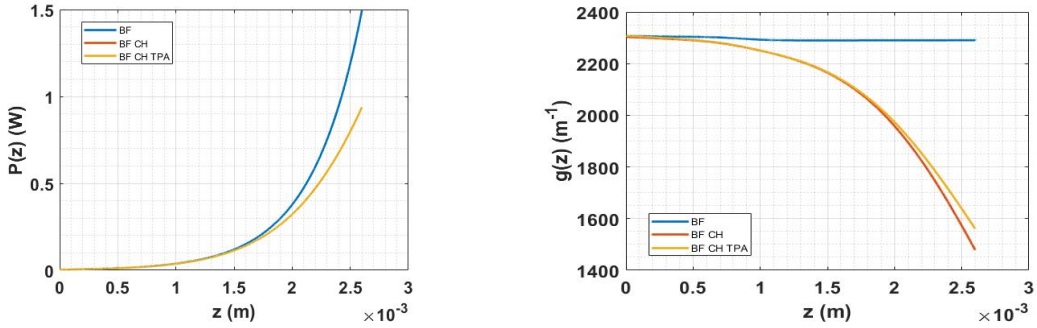

(a) Simulated P(z) (b) Simulated g(z)

Figure 3.15: Power and gain with respect to the length of the SOA (derived model). Note that in 3.15a the red curve has almost the same values as the yellow one, so only one curve can be seen.

presence of nonlinearities (3.16); they almost do not change the behaviour of the gain. In the picture, the output saturation power is plotted ($P_{out,sat} \approx 0.69 P_{sat}$, [1]) defined as the output power for which $G = G_0/2 = e^{h_0}/2$ ([1]).

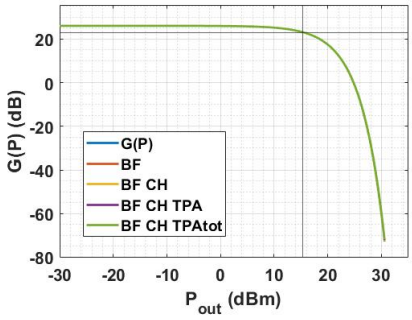

Figure 3.16: Device Gain with output power; solid lines show the value $(P_{out,sat}, G_0/2)$

Chapter 4

Conclusions

The presented work, in the framework of a five months internship, has considered the study of the MOPA as a solid state based source for LiDAR and FSO applications.
The study has been performed on the SCOW structure, considering first a massive slab configuration and then a diluted one, and has given the possibility to have an overview of the different possible configurations that enable the maximization of the device output power; in particular losses in the p-doped region have been decreased considering a 'non-uniform' diluted slab.
Then, a theoretical and numerical study has been performed on the SOA stage, considering the possibility of amplitude and phase modulation. The model simulates nonlinear effects in the semiconductor material consequent to a pump-probe experiment. The nonlinear phenomena of Band Filling, Carrier Heating, Two Photon Absorption and Free Carrier Absorption induced by TPA have been modeled, while Spectral Hole Burning have not been considered both in gain and index dynamics. Material and device gain, phase and index dynamics have been calculated in presence of the effects together with carrier density dynamics. A mathematical model has been derived and simulated, in order to account for nonlinear effects in power and material gain dependence along the length of the device. Results mainly follow literature, even if some discrepancies are present in the pump current considered and in the modeling of the FCA effect. The objective is then to solve these discrepancies, and the presented model will be the base of a following analysis, concerning the frequency behaviour of the device, in which the main goal will be the study of the transmission of the SOA in the frequency domain. Modulation of both pump current and input optical power will be studied with their impact on the transmission of the device. The analysis will also consider the possibility of asymmetrical current pumping (having different currents in the input and in the output part of the device, considering the model of a two section SOA, see [16]). The analysis will start both from integrated gain dynamics and carrier density dynamics, in which the different nonlinearities will be considered. The model will be then compared with experimental results previously obtained on the frequency behaviour of the device, and from this comparison it will be ameliorated in order to better simulate the devices available in the laboratory.

Chapter 5

Appendix

5.1 ALCOR

To simulate the SCOW structures with both massive and diluted slab, the software ALCOR is employed, which is the achronym for 'Aide Logicielle à la Conception des composants Optoélectroniques integRés'. The software calculates the mode shape having as input the layered structure of the waveguide. The equation of propagation of quasi-TE modes is calculated, in a domain of n parallel layers with different refractive index, and this latter is considered to be only dependent on x-direction, which is the one along the width of the waveguide ($n = n(x)$). The modes involved in the propagation equation are decomposed into a series of base functions depending on x, weighted by y-dependent coefficients. The problem is then simplified in solving a ordinary differential equation along y.

5.2 Matlab Code

The implemented Matlab code employed to simulate SOA nonlinearities is based on the numerical solution of differential equations by using the finite differences method, in order to discretize the derivatives, passing from a differential equation to an algebraic one. Both time and space are discretized. In particular only z-direction in space is discretized in order to obtain results all over the length of the device. For the different equations, starting from a general first order ODE:

$$\frac{df(x)}{dx} = af(x) \tag{5.1}$$

where x can be time or space variable (t, z) and f is a function of this variable, while a is a constant, having that $df(x) = f(x + dx) - f(x)$, the infitesimal element dx is taken as:

$$dx = \frac{|x|}{N} = h \tag{5.2}$$

where $|x|$ is the extension of the domain in which variable x is calculated (e.g.: the length of the device, or the time interval of the input signal), and N is the number of elements chosen to discretize the domain. This leads to have dx as very little, but finite value h, giving the possibility to simplify the equation:

$$\frac{f(x + h) - f(x)}{h} = af(x) \tag{5.3}$$

Solving only for $f(x + h)$:

$$f(x + h) = af(x)h + f(x) \tag{5.4}$$

calling $f(x+h) = f_{i+1}$ and $f(x) = f_i$:

$$f_{i+1} = a(f_i)h + f_i \tag{5.5}$$

the latter equation has then to be solved $\forall i \in [0, N]$. For what concerns second derivatives they are discretized following the second order backward discretization:

$$\frac{d^2 f(x)}{dx^2} = \frac{\frac{f(x)-f(x-h)}{h} - \frac{f(x-h)-f(x-2h)}{h}}{h} = \frac{f(x) - 2f(x-h) + f(x-2h)}{(h)^2} \tag{5.6}$$

and, in the same way as 5.5:

$$\frac{f(x) - 2f(x-h) + f(x-2h)}{h^2} = \frac{f_i - 2f_{i-1} + f_{i-2}}{h^2} \tag{5.7}$$

Bibliography

[1] Qiang, Wang. Semiconductor optical amplifiers. World scientific, 2013.

[2] Mecozzi, Antonio, and Jesper Mørk. "Saturation induced by picosecond pulses in semiconductor optical amplifiers." JOSA B 14.4 (1997): 761-770.

[3] Tang, J. M., and K. A. Shore. "Strong picosecond optical pulse propagation in semiconductor optical amplifiers at transparency." IEEE journal of quantum electronics 34.7 (1998): 1263-1269.

[4] Agrawal, Govind P., and N. Anders Olsson. "Self-phase modulation and spectral broadening of optical pulses in semiconductor laser amplifiers." IEEE Journal of quantum electronics 25.11 (1989): 2297-2306.

[5] Mork, Jesper, and J. Mark. "Time-resolved spectroscopy of semiconductor laser devices: Experiments and modeling." Physics and Simulation of Optoelectronic Devices III. Vol. 2399. International Society for Optics and Photonics, 1995.

[6] Marculescu, Andrej, et al. "Spectral signature of nonlinear effects in semiconductor optical amplifiers." Optics express 25.24 (2017): 29526-29559.

[7] Pham, Cécil. Sources laser de puissance à semi-conducteurs à 1,55μm pour transmission en espace libre et applications LiDAR. Diss. Toulouse, ISAE, 2019.

[8] Wang, Jin, et al. "Temporal dynamics of the alpha factor in semiconductor optical amplifiers." Journal of lightwave technology 25.3 (2007): 891-900.

[9] Agrawal, Govind P., and Niloy K. Dutta. Semiconductor lasers. Springer Science & Business Media, 2013.

[10] Coldren, Larry A., Scott W. Corzine, and Milan L. Mashanovitch. Diode lasers and photonic integrated circuits. Vol. 218. John Wiley & Sons, 2012.

[11] Duport, François, et al. "Directly modulated high power semiconductor optical amplifier." 2018 International Topical Meeting on Microwave Photonics (MWP). IEEE, 2018.

[12] Pham, Cécil, et al. "Modulation of Master Oscillator Power Amplifier for Free Space Optical Communications at 1.5 µm." 2018 IEEE Photonics Conference (IPC). IEEE.

[13] Juodawlkis, Paul W., et al. "High-power, low-noise 1.5μm slab-coupled optical waveguide (SCOW) emitters: physics, devices, and applications." IEEE Journal of Selected Topics in Quantum Electronics 17.6 (2011): 1698-1714.

[14] Leisher, Paul O., et al. "Watt-class 1550 nm tapered lasers with 45% wallplug efficiency for free-space optical communication." 2016 International Semiconductor Laser Conference (ISLC). IEEE, 2016.

[15] Rochat, Etienne, et al. "Fiber amplifiers for coherent space communication." IEEE Journal of Selected Topics in Quantum Electronics 7.1 (2001): 64-80.

[16] Mork, Jesper, Antonio Mecozzi, and Gadi Eisenstein. "The modulation response of a semiconductor laser amplifier." IEEE Journal of Selected Topics in Quantum Electronics 5.3 (1999): 851-860.